1 Introduction

1.1 Overview

The primary goal of this work is to describe the results of the third flight of the Multi-Spectral Solar Telescope Array, a sounding-rocket-borne observatory that imaged the solar atmosphere at a variety of extreme-ultraviolet and far-ultraviolet wavelengths. I will begin by discussing the context of the mission, explaining what the solar corona is, what we want to know about it, and why. By section 1.3, I will make the definition of the problem more quantitative by presenting a detailed derivation of the Differential Emission Measure function, which describes the temperature structure of the solar atmosphere. I will also describe how multilayer observations such as those obtained by the MSSTA can be used to constrain the DEM.

Chapter 2 contains an exhaustive account of the calibration of the MSSTA instrument. Each component – multilayer mirrors, filters, and photographic film – is treated individually. Since accurate calibration is critical to interpretation of the results from the MSSTA, I will attempt to make any uncertainties in the instrument calibration as clear as possible. Chapter 2 concludes with the presentation of the instrument temperature kernels, which define how the MSSTA telescopes respond to the coronal DEM.

Chapter 3 is an account of the integration and launch of the MSSTA. Representative images from the dataset are presented, and the resolution and calibration of the data are examined in comparison with similar data from other instruments.

Chapter 4 contains my numerical analysis of the MSSTA data. It begins with the testing of various techniques for DEM reconstruction using simulated data. The stability and uniqueness of these techniques are evaluated. I then apply a forward modeling approach to the MSSTA images

and obtain DEMs representing the full solar disk and selected sub-regions. Finally, I discuss the reliability of these results.

In Chapter 5, the implications of the DEM reconstruction analysis are summarized. Suggestions for additional applications of the MSSTA data, and for improvements to future missions now in the planning stages, are presented. I finish by describing the design of a new sounding-rocket mission based on the MSSTA truss, and scheduled for launch in 2006.

1.2 Background

1.2.1 THE CORONA

It is a minor miracle that the moon appears almost exactly the same size as the sun when viewed from Earth. There is no obvious reason why things should have worked out that way, but the result is that occasionally creatures on the Earth are treated to full solar eclipses, when the moon just blocks the disk of the sun. Early observers generally understood the occurrence of eclipses as evidence of divine displeasure. A more modern reading is that eclipses are evidence of a divine mandate to humanity to study the solar corona.

The corona is a diffuse halo of material that surrounds the sun. As seen during eclipses, it is a faintly opalescent glow, dynamic, structured, and tenuous, that streams out to several times the diameter of the solar disk. We now know that the corona links the sun to interplanetary space; indeed, it can be said that the Earth floats through the extended corona. Certainly the storms and surges of the sun's atmosphere are important components in any understanding our own planet's environment, and as we grow as a species and come to rely on satellites operating above most of the earth's atmosphere, or to venture beyond the protection of that atmosphere ourselves, understanding the corona will become increasingly vital to our future.

Observing the corona from earth is extremely challenging because it is so faint compared to the solar disk. It was a long time before respectable scientists believed that the corona was anything but an optical illusion. Once it became possible to make quantitative measurements of its properties, observers were confronted with a mystery: the presence of spectral lines unlike any seen in an earthly lab. Most attributed these to the presence of a novel element called coronium, but this material appeared to behave in bizarre, unphysical ways. Eventually, Bengt Edlén (Edlén 1945) was able to reconcile the extent and behavior of the corona with its observed spectral features: he discovered that the corona was many times hotter than the surface of the sun, up to

several million degrees Kelvin (the surface is ~6000 K). The mysterious lines come from a diffuse, highly ionized plasma of ordinary elements.

This explanation is almost more confounding than the mystery it solved. How can the corona be hotter than the solar surface? It is as if you held your hand over a stove burner, and found that the air above the burner grew hotter rather than cooler as you pulled your hand away (Golub and Pasachoff 2001). The source of the coronal heating remains something of a puzzle to this day. It is clear that energy is stored in the sun's twisted magnetic field, and that this energy is deposited in the solar atmosphere, but the mechanism that releases that heat and produces the structures and motions that we see is not understood in any amount of detail.

However, the discovery that the corona is hot did open up a new avenue for measuring the corona. At 6000 K, the photosphere emits most of its radiation in the visible and infrared range of the spectrum. Because it is so much hotter than the photosphere, the corona emits vastly more ultraviolet and x-ray light, despite the fact that it is not very dense. By pointing an x-ray telescope at the solar disk, we can black out the photosphere and see the corona without waiting for an eclipse or building an occulting disk. Extreme ultraviolet and x-ray astronomy quickly became the primary techniques for studying the solar atmosphere.

1.2.2 X-RAY SOLAR PHYSICS

Of course, trying to observe in x-rays is a challenging problem on its own. First of all, there is the unfortunate fact (unfortunate, that is, for solar physicists; fortunate as far as most living things are concerned) that the earth's atmosphere absorbs essentially all energetic radiation. Instruments must be carried above the atmosphere. In the 1940s and '50s, scientists began mounting solar x-ray detectors on rockets – first on captured German V-2s, then later on dedicated scientific sounding rockets like the Aerobee – and launching them, taking data during the brief period of the rocket's flight when it was above the absorbing layers of the Earth's atmosphere. As technology progressed to the point where it became possible to put instruments on satellites positioned for continuous monitoring of the sun over many years, the amount of solar data grew

exponentially. Still, the sounding rocket program remains an important test bed for new instrumentation, and has produced invaluable data along the way.

The instruments carried on the first rockets were fairly simple proportional counters, with only enough spatial resolution to verify that their signal was coming from the sun. Actually imaging energetic radiation is much more difficult; it tends to penetrate optics, and bending x-rays enough to focus them is not easy. The classical solution is to use grazing-incidence optics like the Wolter telescope, a thin curved shell that deflects incoming radiation by about a degree to form a focus well behind the mirror. Grazing-incidence telescopes are inefficient due to their extremely small collecting area; furthermore, they are quite sensitive to surface errors, and thus are difficult to construct in such a way that they are capable of producing high-resolution images.

The MSSTA

A breakthrough came with the development of multilayer structures capable of reflecting energetic radiation at high angles of incidence. The advantages of multilayer telescopes over grazing incidence optics are legion. Their effective area is orders of magnitude greater, since conventional telescope optics can be used. They are intrinsically wavelength-selective, producing spectroheliograms rather than broadband intensity maps. (A spectroheliogram is an image of the sun in a narrow range of wavelengths.) And they offer the diffraction-limited resolving power of easy-to-fabricate normal incidence optics. The operation of multilayers is discussed in Section 2.2.1.

Depositing a multilayer structure on a Cassegrain mirror enabled A. B. C. Walker's consortium of Stanford University, Lawrence Livermore National Laboratory and the Marshall Space Flight Center to obtain the first high-resolution normal-incidence EUV image of the solar atmosphere (Walker, Lindblom et al. 1988). Within three years, the Walker group had constructed a sounding rocket payload that carried a suite of 14 multilayer telescopes: Multi-Spectral Solar Telescope Array (Walker, Lindblom et al. 1990). The MSSTA flew successfully in 1991 and 1994, imaging the solar atmosphere in a variety of bandpasses. The success of the MSSTA program and the parallel efforts of the NIXT team (Golub 1989) caught the attention of solar physicists

everywhere, and led directly to a series of satellite missions using similar techniques. In 1995, the Extreme Ultraviolet Imaging Telescope (EIT) was launched on board the Solar and Heliospheric Observatory (SOHO); it soon began imaging the solar disk with an array of four multilayer telescopes. In 1998, it was followed by the Transition Region and Coronal Explorer (TRACE), which obtains stunning high-resolution images and movies in similar bandpasses.

1.3 Measuring the Solar Atmosphere

1.3.1 STATEMENT OF THE PROBLEM

Today, TRACE and SOHO are part of a fleet of spacecraft probing all aspects of the solar atmosphere. Extreme ultraviolet observations of the sun have produced some of the most exciting and beautiful images the world has seen in the last decade. Thanks to a fortunate convergence of advances in materials technology and advances in our physical understanding of the corona, we have been treated to pictures showing vast, elegant plumes of superheated plasma arcing over the solar surface; movies depicting the flash of intense energy released during solar flares and the formation of immense arcades of loops in their wake; and measurements of the ceaseless outflow of the solar wind from the coronal holes near the solar pole. These observations have been part of a revolution in solar physics, a quantum leap forward in our understanding of how the solar atmosphere works. Gone are the models of the chromosphere, transition region and corona as spherical shells sitting on top of each other with energy flowing downward to the solar surface; now we recognize the corona as a forest of ever-shifting, interconnected structures spanning spatial scales from meters to hundreds of Megameters.

However, in spite of the qualitative change in our understanding of the solar atmosphere, quantitative analysis of these results has proven extremely challenging. The most basic properties of the plasma that we see in narrowband spectroheliograms – How hot is it? How dense? How are these structures related to each other? What is the source of their energy? – remain elusive. Attempts to measure such quantities often report inconclusive or contradictory results, depending on the assumptions of the investigator and the technique used to analyze the data. The true potential of multilayer telescopes – their unique ability, not only to discern the fine structures of the corona, but to thoroughly diagnose their energetic state – has not yet been achieved. How much detailed, specific, quantitative information about the state of the coronal plasma can be obtained from a set of calibrated, high-resolution extreme-ultraviolet spectroheliograms? It is the goal of this work to answer that question, both in theory and in practice.

1.3.2 DEM

The data set of an instrument like the MSSTA consists of a large number of pixel values $p_i(\mathbf{x})$, where the index i refers to one of the telescopes in the array and $\mathbf{x}$ refers to a particular point in the image plane. These pixel values consist of measurements of the solar irradiance integrated over the solid angle subtended by the pixel and the wavelength bandpass of the telescope:

(Equation 1) $$p_i(\mathbf{x}) = \int_0^\infty \eta_i(\lambda)\mathrm{d}\lambda \int_{pixel\ \mathbf{x}} I(\lambda, \boldsymbol{\theta})\mathrm{d}\boldsymbol{\theta} \qquad [\text{counts s}^{-1}]$$

Here η_i is the efficiency function of the telescope (its bandpass, in units of pixel counts per unit flux at the aperture).

It is not immediately clear how to invert such measurements to obtain a meaningful description of the state of the emitting plasma. A few limitations are obvious: because all its data are obtained from the same vantage point at nearly the same instant of time, the MSSTA can do little to unfold the distribution of plasma along the line of sight or within the pixel, so all measurements will describe a volume integral of some quantity. Furthermore, because it lacks the spectral resolution to measure the shape of emission lines, the MSSTA is essentially limited to measuring some combination of emission line intensities within that volume. That is, as far as the MSSTA is concerned, the intensity of radiation from any volume element of plasma can be treated as a combination of continuum emission and line emission:

(Equation 2) $$I(\lambda) = I_{cont}(\lambda) + \sum_{X,m,j,k} I(\lambda_{jk}^{X+m})\delta(\lambda - \lambda_{jk}^{X+m}) \qquad [\text{ergs cm}^{-2}\ \text{s}^{-1}\ \text{sr}^{-1}\ \text{Å}^{-1}]$$

The symbol λ_{jk}^{X+m} refers to the wavelength of the transition from excited state k to lower state j by an ion of element X in ionization state m.

We can see that any attempt to use MSSTA data to draw inferences about the physics of the corona will rely on understanding how the conditions in the emitting plasma determine the intensities of the various EUV emission lines (as noted in section 2.4.1, the intensity of the EUV

continuum is negligible for our purposes). This problem is discussed in detail in the astrophysical literature [*e.g.* (Pottasch 1963), (Withbroe 1975), (Sylwester, Schrijver et al. 1980), (Judge, Hubeny et al. 1997)], but it will be helpful to explicitly present the derivation of the basic theory of interpreting line intensities, in order to highlight the assumptions on which it rests.

The line-of-sight integrated intensity of an emission line from an optically thin plasma is

(Equation 3) $$I(\lambda_{jk}^{X^{+m}}) = \frac{hc}{4\pi\lambda_{jk}^{X^{+m}}} \int_{z=0}^{1AU} N_k^{X^{+m}} A_{kj} \mathrm{d}z \qquad \text{[ergs cm}^{-2}\text{ s}^{-1}\text{ sr}^{-1}\text{ Å}^{-1}\text{]}$$

where A_{ij} is the spontaneous transition probability and N_j is the number density of the upper level j. The integral is taken along the line of sight z through the corona to the MSSTA aperture. Here we have already begun making simplifying assumptions:

- **Assumption 1:** The plasma is optically thin everywhere above the photosphere, which is treated as a uniform spherical layer at $z(\boldsymbol{\theta}) = 0$, so we can ignore opacity.

We can write the excited-state population as the electron density times a number of ratios:

$$N_k^{X^{+m}} = \frac{N_k^{X^{+m}}}{N^{X^{+m}}} \frac{N^{X^{+m}}}{N^X} \frac{N^X}{N^H} \frac{N^H}{N_e} N_e$$

Treating each of these factors in turn requires a series of assumptions, which are detailed below.

- **Assumption 2:** The elemental abundance $Ab^X = N^X / N^H$ is constant at all points in the corona, and its value is known. We use the coronal abundances measured by [(Feldman 1992), (Landi, Feldman et al. 2002), (Grevesse and Sauval 1998)].
- **Assumption 3:** The fraction of atoms of element X that are in ionization state $+m$ (the ionization fraction $Ion^{X^{+m}}(T) = N^{X^{+m}} / N^X$) is a known function of temperature. We use the ionization equilibrium calculations of [(Arnaud and Rothenflug 1985), (Arnaud and Raymond 1992), (Landini and Fossi 1991)].
- **Assumption 4:** The fraction of ions X^{+m} occupying state j $Pop_k^{X^{+m}}(T, N_e) = N_k^{X^{+m}} / N^{X^{+m}}$ is constant in time, and is a function only of plasma temperature and density. This is equivalent

to stating that the plasma is in local thermodynamic equilibrium, so that the population of the energy levels can be found by solving a system of linear equations for each ion.

Now we can rewrite the emission line intensity (Equation 3) as

(Equation 4) $$I(\lambda_{jk}^{X+m}) = \int_0^{1AU} G_{jk}^{X+m}(T, N_e) N_e N^H \mathrm{d}z \qquad [\text{ergs cm}^{-2}\ \text{s}^{-1}\ \text{sr}^{-1}\ \text{Å}^{-1}]$$

where we have defined the *contribution function* for the $k \rightarrow j$ transition of the ion X^{+m} as

$$G_{ij}^{X+m}(T, N_e) = \frac{hc}{4\pi\lambda_{jk}^{X+m}} \frac{A_{kj}}{N_e} Pop_k^{X+m}(T, N_e) Ion^{X+m}(T) Ab^X$$

The contribution function contains all of the detailed atomic physics parameters that go into determining line strengths – all the complex calculations that we'd like to avoid worrying about and treat as known quantities. To do so, we need to make still more approximations.

- **Assumption 5:** We assume that the processes affecting the ionization state of an element are separable from the processes affecting the level populations of the ions. This is generally the case if the plasma has sufficiently low density, such that collisional excitation is dominant over ionization and recombination in populating the energy levels. Thus, the level populations are determined entirely by electron and proton excitation rates, and the radiative decay rate A_{jk}.

With this assumption, the rate balance equations that will determine the contribution function depend on knowledge of the statistical weights of the levels of each ion, and the radiative decay rate and electron and proton collision rates for each transition. These values are contained in the CHIANTI database (Dere, Landi et al. 1997), along with the abundance and ionization equilibrium tables cited above and a set of routines that perform the calculation of line contribution functions.

While the line contribution functions depend on both temperature and density, their temperature dependence is much stronger. Indeed, Judge *et al.* (Judge, Hubeny et al. 1997) showed that the density dependences of coronal line contribution functions are so weak that it is nearly impossible to derive reliable information about the density of an emitting plasma from even a large number

of observed line intensities. Therefore, we will approximate the contribution function as a univariate function of temperature by making a final assumption.

- **Assumption 6:** The pressure is constant everywhere in the corona. We use a value of $p = 10^{15}$ K cm^{-3}, thereby eliminating the density dependence of the line contribution functions. In fact, pressure probably varies by a factor of 2-4 over the range of plasma imaged by the MSSTA, but the weak density dependence of the contribution function means that this error should not substantially contaminate the interpretation of the contribution function.

With all the atomic physics now contained in constant-pressure contribution functions $G_{jk}^{X^{+m}}(T)$, which can be calculated with CHIANTI, we can change Equation 4 from an integral along the line of sight to an integral over temperature by defining the *differential emission measure* (DEM):

$$DEM(T) = N_e N^H \frac{\mathrm{d}z}{\mathrm{d}T} \qquad [\mathrm{cm}^{-5}\ \mathrm{K}^{-1}]$$

Note that the DEM is sometimes defined as $n_e^{\,2}\, dz/dT$ by setting N^H/N_e, the hydrogen density relative to the free electron density, to 0.83. This is generally valid for coronal plasmas where hydrogen and helium are completely ionized.

The line intensity now becomes

(Equation 5) $$I(\lambda_{jk}^{X^{+m}}) = \int_0^\infty G_{jk}^{X^{+m}}(T) DEM(T) \mathrm{d}T \qquad [\mathrm{ergs\ cm}^{-2}\ \mathrm{s}^{-1}\ \mathrm{sr}^{-1}\ \text{Å}^{-1}]$$

The DEM describes the temperature distribution of the emitting plasma (it can be interpreted as describing the amount of plasma along the line of sight that is emitting the observed radiation and that has a temperature between T and T+dT). Because this function is the only way in which information about the distribution and state of the solar atmosphere enters into the determination of the emission line intensity, the DEM contains all the information about the corona that it is possible to derive from a set of measured line intensities (subject to the above assumptions).

This is an essential point to keep in mind during any analysis of multilayer images. It implies two very important limitations on such an analysis. First, even if we accept that the 6 assumptions

listed above are valid and, therefore, that the DEM tells us everything we can learn from the observations, simply measuring the function DEM(T) does not tell us everything we might *want* to know about the plasma. It does not explicitly describe the spatial distribution of plasma along the line of sight (though we can draw inferences about how structured the plasma is by examining the DEM); this is a fundamental problem in observations of optically thin plasmas. Nor does the DEM contain diagnostic information about energetic processes like magnetic reconnection, since defining a DEM requires assuming that the plasma is in equilibrium and at constant pressure.

Second, we cannot be sure that the assumptions are valid, or that we have assumed accurate values for those quantities that cannot be measured. Of the above assumptions, number 2 is the most troubling. While we have simply chosen a characteristic abundance value and decreed that it is constant everywhere, Feldman *et al.* (Feldman, Doschek et al. 1999), (Feldman 1992) found that absolute abundances can vary by an order of magnitude throughout the solar atmosphere. Our results are quite sensitive to such disparity, since line intensity is essentially proportional to abundance. The situation isn't quite as bad as it looks: the MSSTA instruments do not probe the full temperature range of the solar atmosphere, and thus will see only a fraction of the total abundance variation. Furthermore, most of the strong emission lines seen by the MSSTA (and essentially all those seen by EIT, TRACE and the AIA) are from ionized iron; therefore, the distortion caused by relative abundance errors is limited. Still, the possibility that abundances vary substantially (conceivably as a function of temperature) along all lines of sight appears to be a substantial source of uncertainty in our analysis. The assumed ionization equilibrium values (assumption 3) may also contain uncertainties as large as a factor of 2, and even the assumption that the plasma ionization states and level populations reflect local thermodynamic equilibrium is questionable in light of the possibility of nanoflare heating of the corona (Parker 1988).

Nevertheless, in spite of all the limitations associated with defining and interpreting the line-of-sight DEM, it remains an essential tool for studying the corona. It is particularly useful as an interface between observation and theory. A theoretical model of a particular structure or region or condition in the corona can be made to specify a temperature distribution; this DEM is then used in Equation 5 to predict emission line intensities, which can be compared with observed line intensities to check the model. Observations of emission line intensities can only distinguish between different models to the extent that those models produce different DEMs, and to the

extent that the data set has sufficient accuracy and temperature coverage to constrain the DEM itself.

Thus, measuring the coronal DEM observationally has been a primary goal of numerous solar physics experiments over several decades. The principal technique for obtaining a DEM is to use a spectrograph to measure a large set of emission line intensities $I(\lambda_{ij}^{X^{+m}})$ – at least 20 lines, and as many several hundred. Then, forward modeling is used to find the function DEM(T) that best reproduces the observations [*e.g.* (Brosius, Davila et al. 1996), (Dupree 1972), (Schmelz, Saba et al. 1999)]. A characteristic result of this technique, using observations by the SERTS rocket (Thomas and Neupert 1994), is shown in Figure 1. The best-fit DEM reproduces the intensity of about half of the observed lines to within the experimental errors (although it is worth noting that the error bars indicate relative errors only. The absolute calibration of the SERTS instrument, and thus the overall normalization of the resulting DEM, is uncertain by a factor of two (Brosius, Davila et al. 1998)). There is an RMS scatter of roughly 20-30%

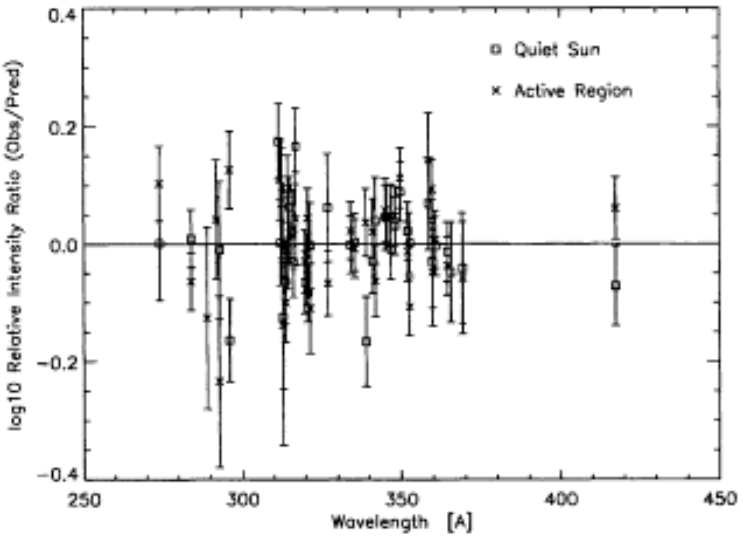

Figure 1. The ratio of intensity predicted by the best-fit DEM to the observed intensity for each of the 26 strong lines used to constrain the DEM. This level of agreement is typical of attempts to extract DEMs from observed spectra. (Figure taken directly from (Brosius, Davila et al. 1996)).

While the scatter is not insignificant, it is small enough to suggest that the assumptions that go into using a DEM are not wildly inconsistent with the reality of the solar atmosphere. Therefore DEMs derived in this way are considered fairly reliable descriptions of the state of the corona

along the observed line of sight. However, there are a number of serious drawbacks to using a spectrograph to measure DEM:

- Field of view: a slit spectrograph has an extremely narrow field of view (only one pixel wide). This can be increased by widening the slit or rastering the spectrograph, but only at the cost of spatial resolution and time resolution;

- Spatial resolution: The best solar EUV spectrographs today – SUMER (Wilhelm, Curdt et al. 1995) and CDS (Harrison, Sawyer et al. 1995) on SOHO, and the SERTS rocket (Thomas and Neupert 1994) – have nominal spatial resolution of 1-10 arc seconds; however, obtaining enough counts in enough lines to measure a DEM generally requires averaging over a much larger area;

- Time resolution: The cadence of these spectrographs is generally on the order of minutes for each pointing; rastering the slit increases the time required substantially;

- Computation time: Finding the DEM that optimizes the fit between predicted and observed line intensities generally takes less than a minute on a fast computer – trivial if only a single DEM is desired, but prohibitive if the DEM is to be found point-by-point over a large field of view with high spatial resolution and time cadence.

In short, spectrographic observations are best suited to measuring a single DEM that describes representative conditions in an average field of view, rather than characterizing particular structures or events. This vagueness, combined with the difficulty of obtaining well-calibrated spectrograms, means that very few temperature-broad, reliable DEMs have ever been measured (the CHIANTI database still makes use of standard "active region" and "quiet sun" DEM functions, which are defined based on averages of spectra taken by (Vernazza and Reeves 1978) in 1973; the well-calibrated observations by the SERTS rocket (Neupert, Epstein et al. 1992) produced single representative active-region DEMs from its flights in 1991 and 1993, which are also widely used).

While deriving DEM in this way is certainly no mean feat, such average DEMs are of limited use. First, averaging emission over a large area increases the likelihood that one or more of the assumptions involved in using a DEM to model that emission will break down. Second, as pointed out in (Aschwanden 2002), observations with a spatial resolution worse than 1 arc second cannot reliably isolate individual coronal loops. Therefore, broadly-averaged DEMs obtained by spectrographs with a resolution of 10-20 arc seconds will never be able to answer fundamental questions about the basic building blocks of the solar atmosphere.

Every time technology has advanced in order to allow us to see the corona with higher resolution, we have found more fine structure and more dynamic phenomena. Clearly the formation and heating of the corona is governed by highly localized processes that take place very quickly; it is impossible to understand the corona without studying it at small spatial scales and with fast cadence. At the same time, a large field of view is also necessary, as the solar atmosphere is both unpredictable and capable of supporting enormous structures spanning hundreds of megameters. Currently, multilayer telescopes are the only instruments that can offer any hope of seeing small details over the full solar disk with a high time cadence.

1.3.3 DEM AND MULTILAYER OBSERVATIONS

Unfortunately, multilayer telescopes, unlike spectrographs, do not return data that can easily be reduced to a tabulated set of emission line intensities. Therefore, it is not trivial to extract a DEM from multilayer observations; quantitative analysis of multilayer images is generally far more limited in scope. However, because the pixel values in a multilayer image (Equation 1) are essentially determined by line emission (Equation 2), and thus by the DEM of the observed plasma (Equation 5), we can attempt to recover a DEM from a set of multilayer observations. The following section describes how multilayer observations depend on DEM.

The Instrument Temperature Kernel

We begin by substituting Equation 2 into Equation 1, setting the continuum intensity $I_{cont}(\lambda)$ to 0, and integrating over all lines of sight that are directed to a particular pixel by the telescope:

$$p_i(\mathbf{x}) = \int_0^\infty \eta_i(\lambda) \sum_{X,m,j,k} I(\lambda_{jk}^{X+m}, \mathbf{x}) \delta(\lambda - \lambda_{jk}^{X+m}) \mathrm{d}\lambda \qquad [\text{counts s}^{-1}]$$

where $I(\lambda_{jk}^{X+m}, \mathbf{x})$ is now the line-of-sight emission line intensity averaged over the pixel. The delta function is an approximation, acceptable here because the widths of the emission lines are smaller by a factor of ~100 than the bandwidths of EUV multilayers; it allows us to write

(Equation 6) $$p_i(\mathbf{x}) = \sum_{X,m,j,k} \eta_i(\lambda_{jk}^{X+m}) I(\lambda_{jk}^{X+m}, \mathbf{x}) \qquad [\text{counts s}^{-1}]$$

That is, the pixel value is just the sum of the intensity of all the coronal emission lines, weighted by the efficiency function of the telescope at the wavelength of the line.

We now substitute the definition of line intensity from Equation 5 into Equation 6, and pull the sum over all lines inside the integral over temperature to write

$$p_i(\mathbf{x}) = \int_0^\infty \sum_{X,m,j,k} \eta_i(\lambda_{jk}^{X+m}) G_{jk}^{X+m}(T) DEM(T, \mathbf{x}) \mathrm{d}T$$

This equation is identical in form to Equation 5 (although here the fact that the variation of intensity along different lines of sight is entirely due to spatial variations in the DEM is made explicit). We can take advantage of the similarity to define a *temperature kernel* function for the instrument:

$$K_i(T) = \sum_{X,m,j,k} \eta_i(\lambda_{jk}^{X+m}) G_{jk}^{X+m}(T)$$

The temperature kernel is simply the sum of the contribution functions of all the lines in the telescope bandpass, weighted by the efficiency of the telescope at the wavelength of each line. With the temperature kernel acting as a sort of multi-line contribution function, we can see that the quantity measured by a multilayer telescope – pixel value – is determined by combining basic

atomic physics with a description of the global state of the plasma in exactly the same way that emission line intensities are determined. That is, we can write

(Equation 7) $$p_i(\mathbf{x}) = \int_0^\infty K_i(T) DEM(T, \mathbf{x}) \mathrm{d}T \qquad [\text{counts s}^{-1}]$$

This suggests that a set of multilayer observations can be used to measure DEM in exactly the same way that spectrograms have been.

The temperature kernel defined above is exactly the same as the instrument response function $R(T)$ described in (Aschwanden, Schrijver et al. 2001), among other places. The function is sometimes calculated by discretizing temperature and sampling at a number of different temperatures T_j, rather than by performing the weighted sum of the line contribution functions. First, a set of spectra $I(\lambda, T_j)$ are generated using discrete isothermal DEMs:

$$DEM_j(T) = D_0 \delta(T - T_j)$$

Then the isothermal spectra are folded through the instrument bandpass to find the instrument's response to plasma at a particular temperature, i.e.

$$K_i(T_j) = \frac{1}{D_0} \int_0^\infty \eta_i(\lambda) I(\lambda, T_j) d\lambda$$

This is the method used by (Weber, DeLuca et al. 2004), among others. It has the advantage of including the effect of the continuum in the isothermal spectra (the continuum is set to 0 in the weighted-sum method). However, the contribution of the continuum is insignificant at EUV wavelengths, and the weighted-sum method is more intuitive and provides more insight into the importance of the various components of an instrument's response.

Chromospheric Instruments

Note that some of the narrowband telescopes carried by EIT, TRACE and the MSSTA probe the chromosphere and lower transition region, rather than the upper transition region or corona. These instruments are not susceptible to temperature kernel analysis because the processes responsible for the bulk of the emission in their bandpasses do not obey the 6 assumptions of

section 1.3.2 (not even in the approximate fashion that we consider acceptable for the coronal bandpasses).

For one thing, chromospheric plasma is not necessarily in LTE (due to ambipolar diffusion, among other effects). More importantly, the opacity of the solar atmosphere is much higher at FUV wavelengths, and at the 304 Å He II line imaged by EIT, than it is at most EUV wavelengths. Therefore, the assumption that the emitting plasma is optically thin is much more likely to break down. Because the line of sight integral for pixels in 1600 Å, 1216 Å, or 304 Å images is more complicated than for other multilayer bandpasses, these chromospheric instruments do not see the same plasma that the other telescopes see, and combining their measurements with those of the coronal telescopes is not straightforward. Furthermore, the far ultraviolet (FUV) emission imaged by the 1216 Å and 1600 Å telescopes on MSSTA and TRACE contains a substantial continuum component. The different observational constraints involved in analyzing FUV and EUV emission are detailed further in section 2.4.1

Observation and analysis of the connection between chromospheric and coronal plasmas has always been a primary goal of the MSSTA (Boerner, Walker et al. 1999); the quality of the chromospheric images obtained in flight ensures that the MSSTA dataset can potentially provide some insight into that connection. However, such analysis is essentially outside the scope of this work.

Requirements for Using Temperature Kernels

It is clear from Equation 7 that multilayer images can provide insight into the coronal DEM at every point on the solar disk in much the same way that spectrographic observations currently do for broadly-averaged regions, provided an adequate set of instrument temperature kernels $K_i(T)$. Of primary importance is the accuracy of these temperature kernels. In the EUV, where a useable instrument temperature kernel can be defined, its accuracy depends on the accuracy of its two ingredients: the bandpass efficiency function of the instrument, and the contribution functions of the relevant emission lines. Obtaining a good measurement of the bandpass efficiency requires detailed knowledge of every component of the instrument. Meanwhile, the line contribution

functions depend on the accuracy of various measured and calculated parameters of the emitting ions, and the validity of the 6 assumptions described in the previous section that go into the definition of the contribution function itself.

Thus, the basic requirements – knowledge of the instrument and of the underlying atomic physics – and the fundamental uncertainties involved in quantitative analysis of line-of-sight emission from an optically thin plasma are the same for both spectrographs and narrowband telescopes. However, using a suite of instruments is a little more complicated than measuring multiple lines from a single instrument. Since each bandpass in a multilayer dataset essentially plays the role of a single emission line, an assortment of bandpasses with accurate temperature kernels is essential to constrain the DEM over a range of temperatures. Maximizing the diagnostic capability of multilayer telescopes demands a dataset consisting of high-resolution images from a large number of separate, well-calibrated bandpasses.

1.3.4 APPLICATIONS OF TEMPERATURE KERNELS

Unfortunately, such a dataset did not exist prior to the flight of the MSSTA III. The most comprehensive narrowband images came from EIT and TRACE, each of which carries three coronal telescopes with bandpasses centered at 171 Å, 195 Å and 284 Å. Images and movies from those satellites have yielded great advances in our understanding of the solar atmosphere; but with only three separate bandpasses, their ability to yield quantitative information about the thermal structure of the corona is severely limited.

Nevertheless, the literature is full of investigations into the temperature of the corona based on multilayer images from TRACE and EIT. The most common approach is the filter ratio method (e.g. (Wheatland, Sturrock et al. 1997), using soft x-ray observations from Yohkoh; (Neupert, Newmark et al. 1998), using EIT 171 and 195 Å images; (Testa, Peres et al. 2002), who combined TRACE 171 and 195 Å data with forward modeling; and [(Aschwanden, Newmark et al. 1999), (Aschwanden, Alexander et al. 2000)], which used all three EIT bandpasses, though never all three at the same time). This technique requires the assumption that the line of sight to a given pixel passes through plasma at a single temperature; in that case, then the ratio of pixel

values $R_{ij}(T)$ in each of two narrowband images i and j is simply a function of that temperature, found by taking the ratio of the instrument temperature kernels:

$$R_{ij}(T(\mathbf{x})) = p_i(\mathbf{x}) \Big/ p_j(\mathbf{x}) = K_i(T) \Big/ K_j(T)$$

For a set of three narrowband observations of a pixel, two independent filter ratios can be measured; the filter ratios for EIT's 171, 195 and 284 telescopes are shown in Figure 1. The filter ratio temperature T_j^i of a pixel is found by inverting $R_{ij}(T)$.

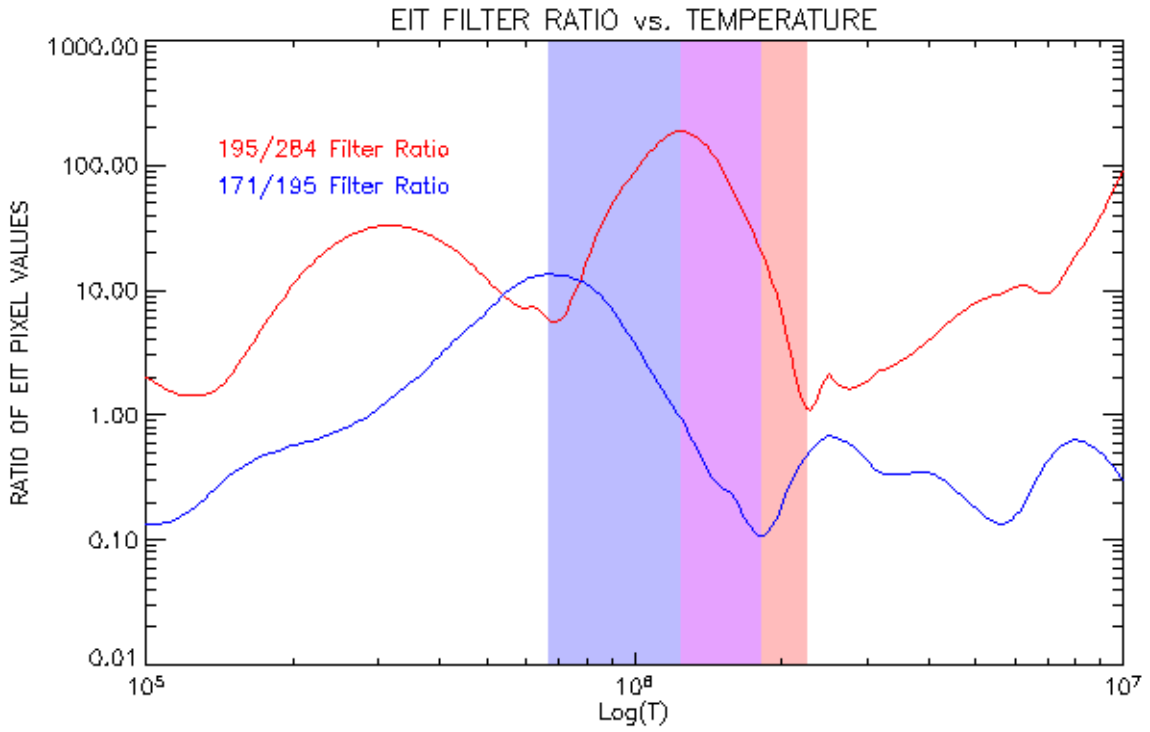

Figure 2. Filter ratios used to measure temperature from EIT observations. The shaded regions indicate the range over which each of the two filter ratios is considered valid (in that the ratio is unique, and each bandpass reasonably responsive). Only in the purple region from T ~ 1.2 MK – 1.8 MK is it possible to obtain two independent measures of plasma temperature.

The numerous drawbacks to the filter ratio method are obvious. First, as illustrated in Figure 1, $R_{ij}(T)$ is seldom a unique function of temperature, so there is generally confusion about the temperature implied by a given filter ratio. Of course, the sensitivity of narrowband telescopes is rather strongly peaked in temperature, so they are unlikely to see substantial contributions from

plasma at a very different temperature from the peak of their bandpass, but still, the difficulty in inverting $R_{ij}(T)$ is inconvenient.

Much more problematic is the assumption of isothermality that must be made before even attempting to measure temperature from a filter ratio. Because the solar atmosphere is highly structured and optically thin at EUV wavelengths, a given line of sight will generally pass through a large number of different plasma elements which are unlikely to be at the same temperature, all of which will contribute to the observed emission. It may be possible, by undertaking painstaking searches for well-isolated loops extending above the solar limb and carefully subtracting the background (Del Zanna and Mason 2003), to find a few pixels whose emission is dominated by a single structure. Even then, however, there is no guarantee that all the plasma along the column-of-sight to that pixel is at the same temperature. As noted in (Martens, Cirtain et al. 2002), the mean free path of electrons in the corona is ~300 km along magnetic field lines, and on the order of centimeters transverse to field lines. Therefore, it must be acknowledged that, even with the best resolution available today – about 1 arc-second, or ~750 km, from TRACE – a particular pixel can contain many separate, thin loop fibrils at different temperatures.

Yet the filter ratio method will always report a single temperature for each pixel. In fact, a given filter ratio always seems to report the same temperature, which is generally midway between the peak response temperatures of the two filters. For example, measurements of the 171/195 Å filter ratio consistently produce temperatures T_{195}^{171} ~ 1.3 MK in a wide variety of structures, and at all points along those structures (e.g. (Lenz, DeLuca et al. 1999) measured four coronal loops at four points each with TRACE's 171 and 195 Å bandpasses; all 16 measurements found the same temperature to within a fraction of the error bars). In the few instances where multiple separate filter ratios have been measured for the same pixel, they do not agree. In (Schmelz, Beene et al. 2003), both EIT filter ratios were measured simultaneously along a number of loops. In all measurements, T_{195}^{171} was ~1.3 MK and T_{284}^{195} was ~1.9 MK for the same pixel.

Assuming that a pixel images isothermal plasma is not only an oversimplification; it will, in general, destroy our ability to extract information about the true temperature structure of the

plasma along that column-of-sight. The DEM of a given pixel contains full information about the distribution of temperatures in that pixel, and can in general be expected to be a broad, complicated function. Requiring the pixel to be isothermal and using a filter ratio to measure a single temperature is not a useful approximation in cases where the pixel actually contains a broad range of temperatures; it does not, say, give insight into the temperature at which the pixel's DEM peaks, or the weighted mean of the DEM. As demonstrated by (Martens, Cirtain et al. 2002), a broad DEM will always produce constant filter ratio temperatures, whose values have more to do with the instruments themselves than with the plasma.

With three bandpasses to choose from, it is not necessary to assume isothermality. Making an isothermal approximation requires two observations to constrain its two variables – temperature, and emission measure at that temperature. With three observations, we can add in more variables, and thereby capture more of the subtlety of the temperature structure. For example, (Zhang, White et al. 1999) constructed a two-component model of the solar atmosphere using four variables – the temperatures and emission measures of the hot and cool components – which they constrained with the three EIT bandpasses and a set of (rather broad) assumptions. While this approach is intriguing, it is badly underconstrained; the technique has difficulty reproducing even conservative (*i.e.* relatively smooth) artificial DEMs, and is highly sensitive to noise. The model results of (Zhang, White et al. 1999) do not constitute a substantially better estimate of the DEM than those obtained from filter ratios.

Indeed, any attempt to measure the temperature structure of even a very well-resolved (half arc-second) pixel by inverting observations in three independent bandpasses is doomed to fail amid non-uniqueness and invalid assumptions. An alternative approach is to use forward modeling to attempt to reproduce the pixel values seen in multilayer images. In this case, rather than try to extract the DEM from the observations, an artificial set of observations is generated from a model of the physical state of the plasma, and compared to the true observations. Then the parameters of the model are adjusted to optimize the correlation between observed and expected pixel values. This technique can be very powerful, and has the advantage that it goes straight to the underlying physics. Rather than attempting to parameterize the DEM in terms of the observations, it allows the investigator to directly tune the actual conditions in the corona – the reconnection rate, say, or the plasma density, or whatever variables allowed by the model – in order to match the data.

For example, (Aschwanden, Schrijver et al. 2001) calculated hydrostatic loop models that were able to reproduce a set of TRACE 171 Å and 195 Å observations. They found that only models of essentially isothermal loops in which the heating of the coronal plasma took place at the base of the loops were able to match the data; loops heated uniformly along their length, or near their tops, produced intensity profiles that were inconsistent with those seen by TRACE. These findings constitute some of the strongest observational evidence to date for the location of coronal heating, and demonstrate how forward modeling can extend the utility of the limited observations currently available.

However, the fundamental limitations that apply to inverting a set of observations are not erased by taking a forward approach to the problem. Forward models must be fairly simple, if they are being compared to a small data set. In particular, loop models generally assume that only one, or perhaps a few, structures contribute to the flux seen by a given pixel; otherwise, the model complexity grows to the point where it has enough flexibility to trivially reproduce any observations. Yet the corona is not simple, and most pixels contain huge numbers of structures. Background subtraction remains essential, but background subtraction is difficult off the limb and nearly impossible at the center of the solar disc. There is no reason to believe that a simple model can accurately describe the flux seen in the vast majority of pixels in a multilayer image.

Furthermore, even in cases where a simple model might reasonably apply, the fact that a particular model reproduces a limited set of observations is not entirely compelling. While the inability of a class of models to reproduce the observations is telling, there is no guarantee that a successful forward model is a unique solution. Even if the optimized parameters of the model satisfy the most rigorous tests of uniqueness, perhaps the model itself is flawed. If another, entirely different model is able to reproduce the same observations equally well, there is no way to distinguish between the two without more observations. Thus the conclusions obtained from forward models must be viewed with caution.

In the case of the loop models of (Aschwanden, Schrijver et al. 2001), it may be premature to conclude that their ability to match TRACE observations only with loops heated at their bases proves that the corona is heated near its interface with the chromosphere. Alternative models,

such as the nanoflare picture of (Cargill and Klimchuk 2004), predict stochastic heating all along the loop; this model leads to multithermal loops whose broad DEM has a roughly power-law slope. The nanoflare model has not yet been tested as rigorously as the base-heated isothermal models (Aschwanden, Schrijver et al. 2001). However, as noted by (Schmelz, Beene et al. 2003), broad DEMs such as those predicted by assuming multi-threaded, uniform-heated loops can produce the constant filter ratios just like those used to constrain the models of (Aschwanden, Schrijver et al. 2001).

Thus some of the central questions in solar physics – are individual coronal loops isothermal or not? Where does the heating of the corona take place? – remain unanswered. What is most frustrating is not simply that they are unanswered, but that different datasets seem to be providing different, but equally clear, answers at the same time. Spectral observations consistently find a broad DEM, implying multithermal loops (probably heated along their length) at even the smallest spatial scales they can see, while highly-resolved narrowband images suggest that loops are isothermal (and thus most likely heated at their footpoints). Proponents of spectral observations suggest, quite correctly, that a set of three narrowband images is insufficient to prove that a given plasma element is isothermal. Proponents of multilayer observations counter, equally correctly, that the poor spatial resolution of the current generation of spectrographs is responsible for the broad temperature distributions they find, while the fundamental loops are only resolved by narrowband imagers.

Clearly, what is needed is a way to obtain detailed temperature information about the corona – much more detailed than what is available from the three EUV bands of TRACE and EIT – at very small spatial and temporal scales – much smaller than those probed by CDS or SUMER. We have already specified that a suite of high-resolution, temperature-separated multilayer bandpasses is desirable. More specifically, though, we now see that we need enough bandpasses that their temperature kernels allow for an accurate measurement of the coronal DEM. The data must be sufficient to constrain the DEM over a broad temperature range, without making any additional assumptions beyond those that go into defining the DEM.

For it is crucial to point out that most forward models of the corona do not get around the uncomfortable necessity of using the DEM and all the dangerous assumptions described in

Section 1.3.2. Generating a set of theoretical observations to compare with the data means asking the physical model to produce a DEM, and using that DEM to predict line fluxes with Equation 5. Therefore, if a technique can be developed to extract an optimized DEM from a set of observations, it can be still be used to constrain forward models. If the DEM extraction technique itself is reliable, flexible, unique and robust to noise, it is the best of all possible worlds: the resulting function contains all the information about the temperature structure of the plasma along a line of sight that can possibly be extracted from a set of observations with temperature-kernel type instruments.

Extracting spatially-resolved DEMs from high-resolution multilayer images is the holy grail of solar EUV observations; it is similar to the pursuit of other holy grails (Malory and Cooper 1998) in that even failure to achieve the final goal can be illuminating. And failure is a possibility: even if we can develop a technique that should be able to recover the DEM from a set of observations, a technique that consistently reproduces artificial data under realistic conditions, we may find that this technique is incapable of recovering a DEM from actual data. There may not be a DEM function that reproduces all the observations of a given pixel to within their experimental errors. In that case, we will have demonstrated (and, indirectly, measured) inaccuracies in either the instrument calibration or the assumptions and parameters underlying our line flux calculations.

The possibility of failure, and the corresponding ability to identify the limits of the data and analysis technique, is the one of the central advantages of using a DEM-extraction approach before attempting any modeling. If a forward model fails to reproduce observations, its failure is generally taken as proof that the physical model itself is invalid. However, since most models rely on producing DEMs to simulate observations, knowing whether there exists a DEM that can reproduce the data is vital to interpreting the results of a modeling effort. If a DEM can be found, the model output can be compared with that DEM before it is checked against the observations. If not, then negative results from forward models can be disregarded, and new observations or assumptions are necessary.

Previous analyses of multilayer observations have been restricted by the limited number of bandpasses to making approximate and rather dubious estimates of the temperature structure of the emitting plasma. Ultimately, their results tend to be either internally inconsistent (as when

multiple filter ratios report different temperatures for the same pixel) or trivial (as when a single filter ratio finds isothermal plasma everywhere). Such findings say more about the assumptions that go into the analysis than they do about the data themselves. Only by extracting a full DEM spanning the range to which the instruments are sensitive, or determining that there is no such DEM capable of reproducing the observations, can we fully realize the temperature diagnostic capability of narrowband instruments.

1.4 Summary

A cartoon summarizing the proposed approach to analysis of multilayer observations is shown in Figure 3. Beginning with raw images of the solar corona, we create a set of calibrated images. Currently, that is where the processing of data from multilayer instruments stops; it is up to each investigator to create a model of the solar atmosphere visible in those images, use that model to predict a DEM, and fold that DEM through the instrument temperature kernels for comparison with the observations (following the red arrows). Instead, we propose to take the path indicated by the blue arrows, and use the calibrated images and knowledge of the instrument temperature kernels to derive a unique DEM that fully describes the state of the coronal plasma. The essential difference between the two approaches is that our proposed path will answer the question of whether any DEM is observable; if it is, it will provide an estimate of how well-constrained that DEM is. The majority of the work conducted with multilayer images has proceeded without this knowledge, and the success or failure of this work to reproduce the observations has lead to conclusions that, upon closer examination, the data do not fully support.

The items in circular icons in Figure 3 all correspond to potential sources of error – statistical noise in the raw images, uncertainties in the calibration measurements on the film, mirrors and filters, and breakdowns in the assumptions or the accuracy of the atomic physics. Whatever path is followed, these errors must be monitored, understood and minimized. In the following chapter, I will explicitly describe my efforts to measure and reduce the calibration errors of the MSSTA III.

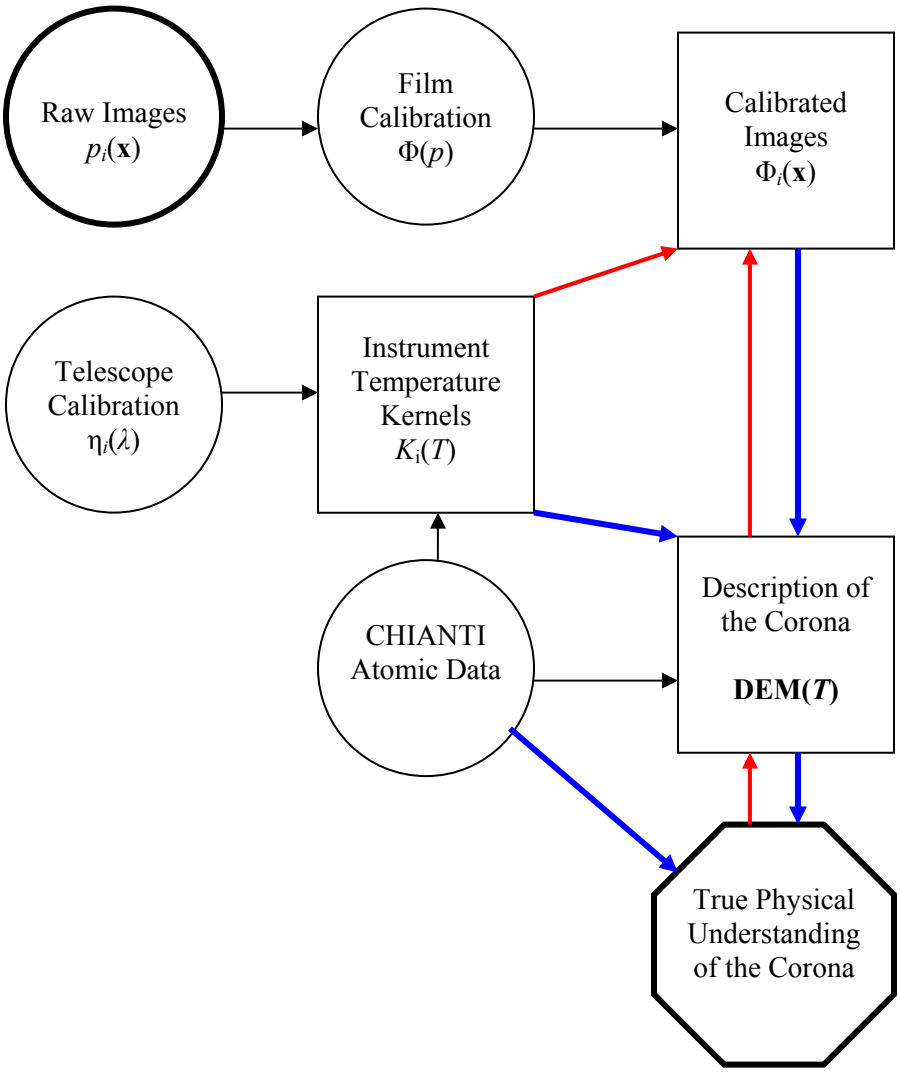

Figure 3. Schematic depiction of how EUV spectroheliograms can lead to a better understanding of the solar atmosphere. Conventional analysis follows the red arrows; we hope to create a more rigorous and streamlined approach following the blue arrows.